Energy 342 (2026) 139660

Contents lists available at ScienceDirect

Energy

journal homepage: www.elsevier.com/locate/energy

Fused portfolio optimization for harnessing marine renewable energy resources

Mary Maceda [a,*], Rob Miller [b], Victor A.D. de Faria [c], Matthew Bryant [a], Chris Vermillion [d], Anderson R. de Queiroz [b]

[a] Mechanical and Aerospace Engineering Department, North Carolina State University, Raleigh, 27606, NC, USA
[b] Civil, Construction, and Environmental Engineering Department, North Carolina State University, Raleigh, 27606, NC, USA
[c] Operations Research Department, North Carolina State University, Raleigh, 27606, NC, USA
[d] Mechanical Engineering Department, University of Michigan, Ann Arbor, 48109, MI, USA

ARTICLE INFO

Keywords:
Renewable energy
Marine energy
Offshore energy
LCOE
Portfolio optimization

ABSTRACT

Offshore wind and marine hydrokinetic energy are underutilized energy resources. Efficiently exploiting these energy resources requires the identification of optimal deployment locations and optimal designs for offshore energy harvesting devices. These devices have the potential to be deployed in tandem such that the suite of devices consistently saturates a given power transmission system. To better understand the economic viability of harvesting marine renewable energy, a portfolio optimization is presented here. Portfolio optimization frameworks help to identify optimal deployment maps for energy-harvesting devices in a given domain and unify solutions of resource, technical performance, transmission, and cost model sub-problems into a unique and comprehensive tool. These frameworks select the energy-harvesting device designs in advance. This work proposes a portfolio optimization framework combined with optimal device design, sizing, and selection to enable a more realistic energy depiction that is beneficial to stakeholders. By maximizing power sent back to shore subject to a constraint on the levelized cost of energy, the algorithm creates an optimal mapping of devices that produces the maximum transmittable power and stabilizes portfolio variability in a cost-effective manner. Any reliably modeled offshore energy-harvesting device can be used within this framework. In this work, wind turbines and marine hydrokinetic kites are selected as a case study considering they are leading technologies for harvesting their respective energies. Results from this case study demonstrate optimal portfolios of devices for a location off the coast of North Carolina and show the utility of fusing device design optimization with the portfolio optimization.

1. Introduction

The ongoing energy transition is rapidly expanding, necessitating the utilization of different renewable energy sources. In this context, marine renewable energy (MRE) resources are presented as promising sustainable energy candidates, which remain largely untapped [1]. Specifically, offshore wind energy has the potential to provide significant amounts of energy should energy-harvesting devices be deployed at scale [2]. Ocean current energy also possesses significant energy potential, provided energy-harvesting devices are deployed at scale [3]. Their energy potential leads to offshore wind and ocean current energy being of particular interest in MRE. Worldwide, the Global Wind Energy Council anticipates an expansion of 380 GW of wind capacity by 2032 [4]. Domestically, by 2040 policies in the United States (US) anticipate an offshore wind capacity of 42,730 MW, which is a 9% increase from 2022. [5]. Additionally, using ocean current as an energy resource has the technical potential to produce 2300 TWh/yr energy along the entire US coast [6]. Furthermore, the Gulf Stream between Florida and North Carolina (NC) has the potential to produce 49 TWh/yr of energy, which equates to about 207 million homes [7].

NC in particular is focused on developing legislation and infrastructure to support utilization of the readily available MRE resources off of their coast. In 2021, NC passed legislature committing to reduce statewide CO_2 emissions by 70% by 2030, and become carbon neutral by 2050 [8]. Considering NC's location, especially with regard to the Gulf Stream, it has the potential to utilize offshore energy resources to aid in achieving carbon neutrality [9].

Harvesting these offshore energy resources, especially ocean current energy, in addition to the wind resource enables maximization of

* Corresponding author.
E-mail address: memaceda@ncsu.edu (M. Maceda).

https://doi.org/10.1016/j.energy.2025.139660
Received 4 August 2025; Received in revised form 1 November 2025; Accepted 10 December 2025
Available online 12 December 2025

energy output as well as increases the cost-effectiveness of energy harvesting [10]. To compete with fossil fuels, coordinating energy generation from these resources needs to be cost-effective. Portfolio optimizations are a tool that can be used to assess the economic viability of a given portfolio (for this work, of energy harvesting devices).

Portfolio optimizations were pioneered in the field of economics when Harry Markowitz published his mean-value portfolio (MVP) theory [11]. His work focused on economics and creating a diversified financial portfolio with the lowest possible risk [12]. Authors have built upon MVP theory and used it to develop portfolio optimization models within the renewable energy field. For example, in [13], portfolio theory was used to reduce economic risk for a given value of economic return for investments into different combinations of renewable energy assets. Similarly, in [14], a portfolio optimization model was used to investigate investment risks and their relation to costs of energy generation when integrating renewable energy into the grid. Additionally, in [15], a portfolio optimization was used to determine the optimal renewable energy portfolios based on risk and profitability under different cost scenarios. A portfolio optimization which addressed deep uncertainty in energy costs was used in [16] to highlight the utility of incorporating renewable energy into the grid and provide energy-management insights. Moving towards offshore energy, in [17] a portfolio optimization method was used in order to select site locations for energy-harvesting devices while reducing the risk of having their production affected by ocean current meander. Furthermore, in [18], a portfolio optimization model was developed in order to reduce the variability in energy delivered back to shore from offshore energy harvesting. From this, it was found that integrating multiple energy-harvesting devices leads to economic benefits and less variability in energy being harvested for a given site [18]. This was further confirmed in [10], where a neural network model was combined with a portfolio optimization model that was designed to reduce the risk within energy generation portfolio. Additionally, in [19], a portfolio optimization was used to explore benefits from shared offshore energy-harvesting device moorings, and mooring optimization.

Previous literature related to offshore portfolio models did not address device design optimization or selection. This necessitates the development of a fused portfolio optimization algorithm as a tool to enable the optimal integration and deployment of multiple energy-harvesting devices for a region of interest. Specifically, this work builds on the framework developed in [18] by (i) Fusing optimal device design, sizing and selection with the portfolio optimization, (ii) taking curtailment of energy into account, and (iii) maximizing the energy sent back to shore as the objective instead of reducing energy variability. Overall, these contributions enable a more realistic energy depiction, which benefits stakeholders. To demonstrate the benefits of the proposed fused portfolio optimization, a case study is performed for a domain off of the coast of NC. For the case study in this work, offshore wind turbines were selected as one of two candidate energy-harvesting devices to input into the portfolio optimization model since wind turbines have been proven to be a leading technology in terms of harnessing available offshore wind energy [20]. Moreover, NC is actively expanding its offshore wind energy harvesting [21]. As mentioned above, NC is located near the Gulf Stream, which provides a consistent ocean current. For this reason, the second candidate device selected for the case study in this work is the marine hydrokinetic (MHK) kite.

MHK kites are the leading technology for harvesting tidal and ocean current energy, and are currently commercially deployed by Minesto [22]. MHK kites use high lift-to-drag wings to fly in specific patterns perpendicular to the oncoming flow. As shown in [23], this enables kites to reach velocities 5 to 10 times faster than the oncoming flow, which allows them to harvest an order of magnitude more energy than stationary turbines. Models for grid-scale MHK kites, such as the Minesto Dragon Class, are not transparent; detailed information about rated flow speeds, ideal operating depths and/or altitudes, rated power, mass, or costs associated with the devices are unattainable [24]. The lack of transparency with existing models necessitates the development of an accurate, open source kite model that can create kite designs for a variety of operating sites such that these designs can be input into the overall portfolio optimization model. Designs for MHK kites can be generated site-specifically, [25]. However, this technique has drawbacks. At a large scale, designing a kite for each individual location would be unrealistic to manufacture based upon impractical tooling costs associated with so many different device designs. Instead, addressing spatial variation in MRE resources by site can be accomplished by creating an optimized suite of kite designs based upon a set number of current speeds and deployment depths that may be encountered within the selected domain. This suite is then input into the portfolio model.

Overall, this work enables the coordination of energy generation from multiple offshore energy sources via a multitude of candidate devices. The contributions of this paper are as follows:

i A fused portfolio optimization model, within which device design, sizing and selection are integrated into an existing portfolio optimization model. This model takes in suites of optimally designed energy-harvesting devices, decides which device designs are the best fit for the domain of interest, and from these, decides the optimal locations and combinations of devices such that power delivered to shore from the transmission system is maximized for a given levelized cost of energy (LCOE) constraint.
ii A transparent MHK kite optimization model
iii Provides a thorough analysis of a real-world case study

The remainder of this work is structured as follows. Section 2 provides descriptions of the fused portfolio optimization model and the design optimization model, as well as in-depth descriptions of the candidate technologies considered in the fused portfolio model and LCOE. Section 3 provides information and details regarding the performed case study. Section 4 provides the results from the case study, and a thorough discussion of the results. Section 5 provides the conclusions of the case study.

2. Fused portfolio optimization model

The fused portfolio optimization in this work is designed to take in data from an environment, candidate energy-harvesting device models, a transmission model, and cost models, and output the optimal deployment configuration of energy-harvesting devices within a given domain. This framework takes optimal device design, sizing, and selection into account. This framework is shown in Fig. 1.

2.1. Model input data

This subsection discusses the input data for the portfolio optimization model including the environmental data used, the covered domain, and how costs will be quantified. The transmission costs are discussed in Section 3.

The wind speed data considered in this work comes from the NREL Wind Toolkit [26]. The ocean current data comes from the Hybrid Coordinate Ocean Model (HYCOM) for ocean current data [27]. Data from the years 2009–2013 was used for this work due. Newer datasets were not used due to the lack of availability of easily accessible ocean current data for the domain.

The domain for the fused portfolio optimization can be made as large or small as desired, provided energy resource data is readily available. This model considers the site-dependency of transmission system costs and the impact of site-dependency of the costs and power outputs of energy-harvesting devices due to the available energy resource. To account for these site dependencies, LCOE, in dollars per megawatt hour, is considered. LCOE is a measure of the lifetime costs

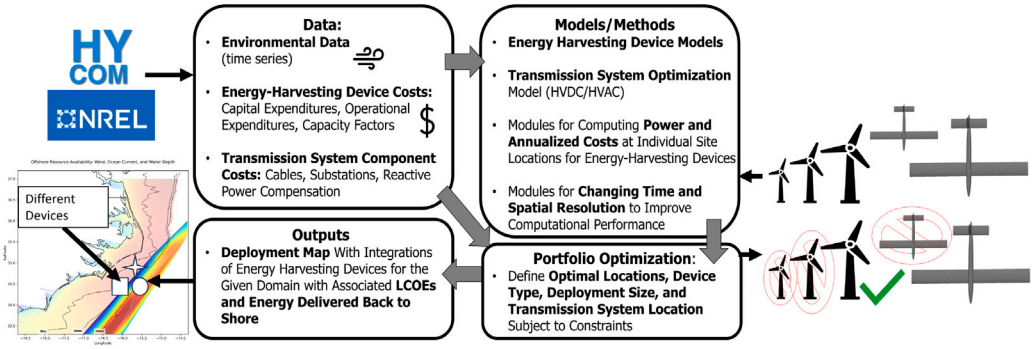

Fig. 1. Overall framework of the portfolio optimization model that shows how the environmental data, energy-harvesting device costs, and energy-harvesting device models interact with the portfolio optimization model.

of a system divided by the lifetime energy production of the system, and is commonly used for economic analysis for marine energy converters [28]. For example, in [29], LCOE is used for design analysis of various devices. Additionally, in [30] LCOE is used to determine the economic feasibilities of offshore energy harvesting deployments.

The lifetime costs of the system are split into capital expenditures and operational expenditures. Capital expenditures include device design, manufacturing, and deployment, and are typically one-time costs for the system. Conversely, operational expenditures cover yearly expenses such as maintenance and leasing costs. These will be defined for each candidate device and the transmission system in Section 3.

2.2. Candidate technologies

Coordination of energy generation methods through a portfolio optimization requires reliable models of energy-harvesting devices and transmission systems. For energy-harvesting devices, the discussion in this paper focuses on models for wind turbines and MHK kites. This subsection will provide insight into these wind and kite system models.

2.2.1. Wind turbine modeling

Since wind turbines are an established technology, wind turbine models are readily available. This work uses reliable wind turbine models from the NREL 2023 Annual Technology Baseline (ATB) [31]. Models for 8 MW turbines (typical 2021 design) and 12, 15 and 18 MW turbines which are esimated to represent offshore wind deployments in 2030 considering respectively a conservative, moderate and advanced development of the offshore wind energy sector. These wind turbines are shown in Fig. 2 along with their associated rotor diameters and hub heights. To solve for the power the wind turbines produce at a given wind speed, power is solved for based on the wind speed at a given site based on the power curves shown in Fig. 3 which follow the power law shown in Eq. (1). Here, ρ is the air density, A is the swept area of the wind turbine blades, C_p is the coefficient of power of the turbine, and v_w is the wind speed at the hub height of the turbine. Note that the C_ps for each wind turbine at various wind speeds are given along with their designs in [31].

$$P = \frac{1}{2}\rho A C_p v_w^3 \tag{1}$$

2.2.2. Marine hydrokinetic kite modeling and design suite optimization

MHK kites (kites) are one of the candidate devices included in the portfolio optimization. Kites were selected for this case study because they are a leading technology for harvesting ocean current energy [32]. As discussed in Section 1, a kite's high lift-to-drag ratio allows it to "fly" underwater at speeds significantly in excess of the prevailing flow speed, which through the cubic relationship between flight speed and power easily leads to an order of magnitude increase in power per unit area when compared to stationary systems [23]. An example kite deployment is shown in Fig. 5. As with wind turbines, the portfolio optimization requires a characterization of the techno-economic performance of a suite of kites. However, unlike with wind turbine manufacturers, leading underwater kite manufacturers like Minesto [24] do not provide comprehensive power curve and cost data for their designs (e.g., the Minesto Dragon Class), and the designs themselves have not been tailored to the target region of operation for our studies. Because of this, prior to performing the portfolio optimization, a family of kite designs and corresponding performance characterizations were generated, using an in-house model and optimization procedure. Specifically, a suite of kites were optimized based upon Eq. (2):

$$\begin{aligned} &\text{maximize} && P(\bar{u}, v_r) \\ &\text{subject to} && h(\bar{u}, v_r) = 0 \\ & && g(\bar{u}, v_r) \le 0 \end{aligned} \tag{2}$$

where P represents power, $\bar{u}$ represents the vector of design variables, v_r represents the flow speed for which a particular set of variables were optimized (termed the *rated* flow speed), $h(\bar{u})$ represents the set of equality constraints, and $g(\bar{u})$ represents the set of inequality constraints. The decision variables are given in Table 1. It is important to note that, although the objective function purely incentivizes power without any penalty for cost (or a surrogate, such as mass), bulky and costly systems are ultimately disallowed through constraints that require sufficiently low mass.

Table 1
Kite decision variables.

Variable	Meaning	Units
s	Wingspan	m
AR	Aspect ratio	–
D	Fuselage diameter	m
L	Fuselage length	m
t_{sh}	Thickness of wing shell	m
t_{sp}	Thickness of wing spars	m
t_{fs}	Thickness of fuselage	m

To complete this optimization, reliable and transparent models for both power output and constraints are needed. In the following subsections, these will be discussed, starting with the power model.

Power model: The central goal in generating a family of kite designs is to perform the optimization of (2) for multiple values of rated flow speed, v_r. The kites in the work are fly-gen systems, and as such, produce power through onboard turbines attached to their wings [33]. Assuming the fuselage produces no lift, for a given set of operational variables and marine deployment, the kite's power output at v_r is calculated according to Loyd's ideal assumptions [23]. This ideal power output model is conventionally used in kite systems [34]. Moreover, it

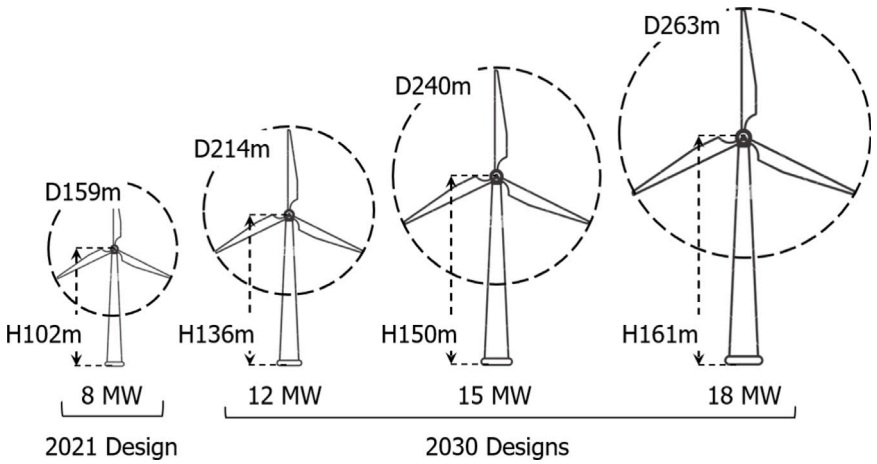

Fig. 2. 8, 12, 15, and 18 MW wind turbine designs from [31] with associated hub heights and diameters.

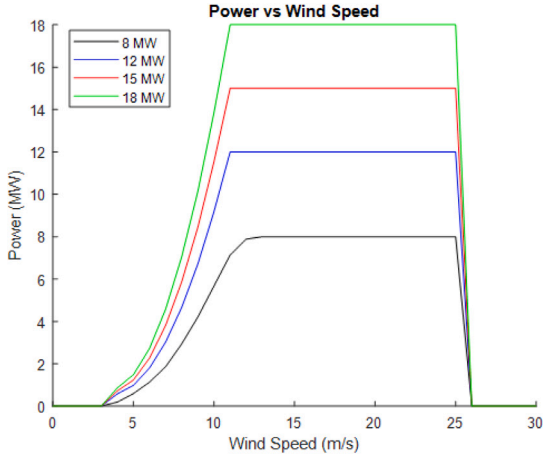

Fig. 3. 8, 12, 15, and 18 MW wind turbine power curves from [31].

has been experimentally validated for MHK kites [35]. This model is shown below in Eq. (3):

$$P(s, AR, L, D) = \frac{2}{27}\rho_{H_2 0} S_w(s, AR) V_r{}^3 \frac{C_L^3(s, AR)}{C_D^2(s, AR, L, D)} cos^3(\theta) \tag{3}$$

where $\rho_{H_2 0}$ is the density of water, S_w is the planform area of the wing, V_r is the rated flow speed of the kite, C_L is the kite's lift coefficient, C_D is the drag coefficient of the system and θ is the optimal elevation angle. It should be noted that the drag coefficient is inclusive of terms for both the kite drag and the drag on the tether. Longer tether lengths result in more drag, slowing the kite's velocity and resulting in power losses [36]. Furthermore, for maximum power, the kite is considered to be flying at the optimal angle of attack (AoA), which is defined as the AoA that maximizes $\frac{C_L^3}{C_D^2}$ [37]. For additional information on the calculations of C_L, C_D, and S_w, the reader is directed to [38]. The variables s, AR, L, and D are the wingspan, aspect ratio, fuselage length and fuselage diameter of the kite respectively. These four variables will be referred to as the geometric variables, and are the only decision variables that affect the power output of the system (the other variables affect constraints but not power).

Constraint models: The constraints of Eq. (2) come in the form of (i) a neutral buoyancy inequality constraint (which imposes an upper limit on mass), (ii) an equality constraint on fuselage thickness that ensures appropriate shear stress and bending moment (although this can be written as an inequality constraint, it will always be active), and (iii) an inequality constraint on the wing's tip deflection.

The neutral buoyancy constraint requires that the *structural mass* of the kite fall below a prescribed fraction of the mass of displaced water. By setting this fraction substantially lower than unity, reserve mass becomes available for ballast and additional payloads that do not contribute to satisfying structural constraints. The kite's structural mass is characterized based on the fuselage's structural mass (given by m_f and including the tail) and the wing's structural mass given by (m_w), with the constraint given by:

$$m_f(s, AR, t_{sh}, t_{sp}) + m_w(s, AR, L, D, t_{sh}, t_{sp}) \leq \gamma m_{disp}, \tag{4}$$

where m_{disp} is the displaced mass of water. In addition to the straightforward process of computing the displaced volume (and therefore m_{disp}), it is clearly necessary to calculate the structural mass terms.

The wing mass is calculated as [39]:

$$m_w(s, AR, t_{sh}, t_{sp}) = s\rho_w[A_{sh}(s, AR, t_{sh}) + A_{sp}(s, AR, t_{sh}, t_{sp})] + \rho_{fm} m_{fm} \tag{5}$$

where A_{sh} is the total area of the wing shell, A_{sp} is the total area of the spars, and m_{fm} is the mass of buoyant syntactic foam that fills the empty space within the wing. The buoyancy of the foam allows the optimized kites to achieve neutral buoyancy. Additionally, the wing is assumed to have a constant cross section and the wing's shell and spar thicknesses are assumed to be constant. Furthermore, the wing is assumed to be rectangular. Solving the equation for AR from Fig. 4 for the chord C yields Eq. (6)

$$C = \frac{s}{AR} \tag{6}$$

The fuselage is treated as a thin-walled hollow cylinder, with constant wall thickness t_{fs}. The mass of the fuselage is modeled as [39]:

$$m_f(s, AR, L, D, t_{sh}, t_{sp}) = 2\rho_w \pi D L t_{fs} \tag{7}$$

The second set of constraints are structural limits on the fuselage. Ultimately the fuselage must be sufficiently thick to satisfy both shear stress and bending limits. Because there is no benefit to further thickening the fuselage, both constraints are solved for at equality, then the fuselage thickness, t_{fs}, is set to the larger of the two values (thereby satisfying both constraints). This process is laid out below:

(i) To satisfy shear stress along the wing-fuselage attachment:

$$t_{fs}(s, AR, L, D) = \frac{F_{wing}(s, AR, L, D)}{C\zeta\sigma_{yield}} \tag{8}$$

where F_{wing} is the lift force on the wing's halfspan, ζ is the factor of safety, which is two in this work, and σ_{yield} is the yield strength of

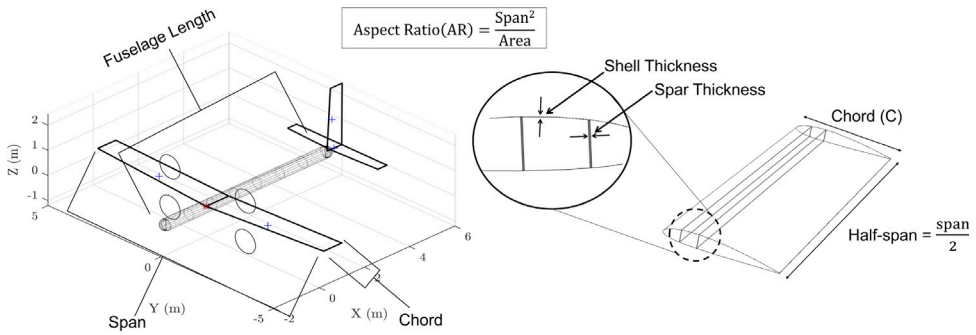

Fig. 4. View of the kite and wing structures, with selected dimensions highlighted.

the material, which for this study is aluminum 6061. This calculation assumes the wing spars are continuous, and thus go through the fuselage. Additionally, it is assumed that the fuselage must be thick enough to account for the shear from both halfspans of the wing. For more information on calculating F_{wing}, see [40].

(ii) To satisfy the bending loads on the fuselage:

$$t_{fs}(s, AR, L, D) = \frac{4|M_{max}(s, AR, L, D)|}{\pi D^2 \zeta \sigma_{yield}} \tag{9}$$

where $|M_{max}|$ is the maximum internal bending moment along the fuselage where the force from the tail is assumed to equal $0.1 * F_{wing}$ acting in the opposite direction as the lift from the wing. The tether is considered to have its attachment points at 40% of the fuselage length. For information on how to calculate maximum internal bending moments, the reader is directed to [41].

The final constraint is an inequality constraint on wing tip deflection. Specifically, to acquire values for t_{sh} and t_{sp}, the wing tip deflection constraint from [39] is considered. The halfspan is treated as a cantilevered beam with a uniformly distributed load. and the maximum wing tip deflection is assumed to be 5% of the halfspan. Following [39]'s solution for the maximum deflection leads to an inequality constraint on bending moment of inertia of the wing, which takes the following form:

$$I_{wing}(s, AR, t_{sh}) \geq I_{required}(s, AR, L, D) = \frac{F_{wing}(s, AR, L, D) * s^3}{\delta * E * 64} \tag{10}$$

where I_{wing} is the moment of inertia (MOI) of the wing, $I_{required}$ is the required MOI of the wing to satisfy the prescribed wing tip deflection limit, δ is the wing tip deflection, and E is the elastic modulus of the wing's material. Solving this at equality for a given t_{sp} allows for t_{sh} to be solved for at equality.

Optimization results: In this work, the optimization of Eq. (2) was solved for rated flow speeds in increments of 0.25 m/s, ranging from 0.5 m/s to 2.75 m/s, which are representative of the section of the U.S. Gulf Stream and shelf under consideration in this work. A grid search over geometric variables, along with a nested line search across spar thicknesses and direct calculation of remaining structural variables (based on equality constraints), was used to perform the optimization. The optimized kite designs and associated power outputs and structural masses for the given design space of operational variables are given in Table 2 (to save space, only span and aspect ratio values are shown, as these exhibit the most notable trends). For a detailed explanation of these results please see Appendix A.

2.2.3. Transmission model

This works incorporates two modes of transmission, both with full reactive power compensation: high voltage direct current (HVDC), and high voltage alternating current (HVAC). The energy losses from the system are divided into offshore terminal losses, losses on cables, and onshore terminal losses. The models for these were taken from [18] and the reader is directed there for more information.

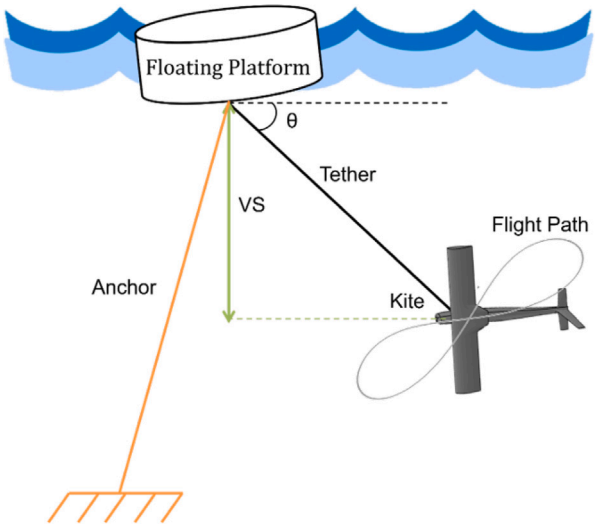

Fig. 5. Floating platform deployment of MHK kite with key mechanical components, VS, and elevation angle, θ, shown.

To optimize the transmission system, an algorithm was developed using the models from [18] to find the optimal transmission parameters out of all possible configurations with the objective being to minimize cost for any given location. These costs will be defined in Section 3.2. To account for anchoring, a maximum depth of 2500 m was used [29]. Line designs with rated powers of 300, 600, 1000, and 1200 MW were considered and the lines were assumed to be operating at a 50% CF. Based upon offshore wind energy deployments, the annualized costs of energy losses was taken to be 83.3 $/MWh [31].

2.3. Portfolio optimization model formulation

This subsection details the portfolio optimization model. The portfolio optimization acts in the following manner: (i) Suites of optimally designed energy-harvesting devices are input into the optimization framework (ii) The model then decides which device designs are the best fit for the domain of interest (iii) From the best fit energy-harvesting devices, the portfolio optimization decides the optimal locations and combinations such that power delivered to shore from the transmission system is maximized for a given levelized cost of energy (LCOE) constraint.

This optimization model treats the following as decision variables: (i) the variable that controls the center of the energy collection system for each possible configuration of candidate energy-harvesting devices, v_i (ii) the relaxation variable for that center w_d, and (iii) the number of energy-harvesting devices of design type d at the site location i, $y_{i,d}$. As previously mentioned, the portfolio optimization model's objective is to maximize energy delivered to shore from a configuration

Table 2
The power outputs, structural masses, spans, and ARs of the optimized kite designs for the design space of operational variables.

Kite parameters										
Rated flow speed (m/s)	0.5	0.75	1	1.25	1.5	1.75	2.0	2.25	2.5	2.75
Power output (kW)	53.7	147.5	312.6	570.8	931.9	1431.6	2041.2	1987.7	1872.0	1814.4
Structural mass (kg)	1780.6	2442.2	3262.0	3738.6	4822.5	5248.7	5682.4	4063.3	2784.8	2101.5
Span (m)	11.0	11.0	11.0	11.0	11.0	11.0	11.0	9.7	8.3	7.4
Aspect ratio	5.3	4.6	3.8	3.8	3.0	3.0	3.0	3.0	3.0	3.0

of energy-harvesting devices. This metric is appropriate because the goal of integrating multiple energy-harvesting devices into a single deployment is to take advantage of being able to harvest multiple energy resources, thereby increasing the amount of energy produced. The objective function that represents this is shown in Eq. (11), where EG_t is the average energy generation for the years of analysis at time t (i.e., each hour) by an energy-harvesting device, Δ_t is the energy curtailed due to limits in the transmission system at time t, and T is the years of analysis. This objective function is subject to various constraints which will be discussed in this section.

$$\max_{y,w,v} \sum_{t\in T} \left(EG_t(y,w,v)^{Wind} + EG_t(y,w,v)^{Kite} - \Delta_t(y,w,v) \right) \tag{11}$$

Within the portfolio optimization, an LCOE (acting as a budget) is set as a constraint, as shown in Eq. (12) where TAC is the total annualized cost of each deployment and TC is the annualized cost of the transmission system. A configuration of devices and device locations is chosen that meets the set LCOE.

$$\frac{TAC^{Wind} + TAC^{Kite} + TC}{8760\ \mathbb{E}_{t\in T}\left(EG_t^{Wind} + EG_t^{Kite} - \Delta_t\right)} \le \overline{LCOE} \tag{12}$$

Next, constraints on aggregating costs are shown in Eqs. (13)–(15) where AC is the annualized cost of deploying one device at a given site location, TC_i is the annualized cost of a transmission system placed at site i, D is the set of device designs, I^d is the set of viable site locations for the deployment of device design d, and I_{Tr} is the set of locations for the energy collection system.

$$TAC^{Wind} = \sum_{d\in D_{Wind}} \sum_{i\in I^d_{Wind}} AC^{Wind}_{i,d}\ y^{Wind}_{i,d} \tag{13}$$

$$TAC^{Kite} = \sum_{d\in D_{Kite}} \sum_{i\in I^d_{Kite}} AC^{Kite}_{i,d}\ y^{Kite}_{i,d} \tag{14}$$

$$TC = \sum_{i\in I_{Tr}} v_i TC_i \tag{15}$$

These constraints determine the total cost of the energy-harvesting devices and the total system costs. This constraint is appropriate because aggregate costs that are exceedingly expensive would deter integrated deployment.

The aggregating energy generation constraints in Eqs. (16)–(17) focus on the total energy generation coming from the energy-harvesting devices (EG_t).

$$EG^{Wind}_t = \sum_{d\in D_{Wind}} \sum_{i\in I^d_{Wind}} EG^{Wind}_{i,d,t}\ y^{Wind}_{i,d} \qquad \forall\, t \in T \tag{16}$$

$$EG^{Kite}_t = \sum_{d\in D_{Kite}} \sum_{i\in I^d_{Kite}} EG^{Kite}_{i,d,t}\ y^{Kite}_{i,d} \qquad \forall\, t \in T \tag{17}$$

The constraint on curtailment is shown in Eq. (18), where RP_{Tr} is the rated power capacity of the transmission system. This constraint balances energy generation and the amount of energy that must be curtailed by the system. Additionally, it considers the balance between creating enough energy to saturate the transmission system, while not over-producing energy to the point where the majority of energy created is being curtailed.

$$EG^{Wind}_t + EG^{Kite}_t - \Delta_t \le RP_{Tr} \qquad \forall\, t \in T \tag{18}$$

Limits on the number of device designs are set in Eqs. (19)–(22) where $\bar{NT}$ is the maximum total number of devices deployed and $\bar{ND}$ is the maximum number of different designs from the given suite of designs used by the portfolio optimization model. These constraints dictate how many different models of each energy-harvesting device the portfolio may choose from.

$$\sum_{i\in I^d_{Wind}} y^{Wind}_{i,d} \le w^{Wind}_d\ \bar{NT}^{Wind} \qquad \forall d \in D_{Wind} \tag{19}$$

$$\sum_{d\in D_{Wind}} w^{Wind}_d \le \bar{ND}^{Wind} \qquad \forall d \in D_{Wind} \tag{20}$$

$$\sum_{i\in I^d_{Kite}} y^{Kite}_{i,d} \le w^{Kite}_d\ \bar{NT}^{Kite} \qquad \forall d \in D_{Kite} \tag{21}$$

$$\sum_{d\in D_{Kite}} w^{Kite}_d \le \bar{ND}^{Kite} \qquad \forall d \in D_{Kite} \tag{22}$$

Limits on the maximum number of devices per site are set by the constraints shown in Eqs. (23)–(24) where $ROL^{A|B}$ is the ratio of the area of the site of the technology A that is overlapped by the site of the technology B, PD is the maximum packing density for each device, $SL^{A|B}$ is how many devices of type A can be placed at the same location for each device of type B and $OL^{A|B|}_{i,d}$ is the set of site/designs (i,d) from technology B that overlap with the sites/designs of technology A. These constraints ensures devices will not overlap or act detrimentally towards one another.

$$y^{Wind}_{i,d} \le \bar{NT}^{Wind}_{i,d} - \left[\sum_{(i_o,d_o)\in OL^{Wind|Wind}_{i,d}} \left(\frac{1/PD^{Wind}_{i_o,d_o}\ y^{Wind}_{i_o,d_o}\ ROL^{Wind|Wind}_{(i,d)|(i_o,d_o)}}{1/PD^{Wind}_{i,d}} \right) - \sum_{(i_o,d_o)\in OL^{Wind|Kite}_{i,d}} \left(y^{Kite}_{i_o,d_o}\ ROL^{Wind|Kite}_{(i,d)|(i_o,d_o)} \left(\frac{PD^{Wind}_{i,d}}{PD^{Kite}_{i_o,d_o}} - SL^{Wind|Kite}_{(d)|(d_o)} \right) \right) \right] \qquad \forall\, d \in D_{Wind}, i \in I^d_{Wind} \tag{23}$$

$$y^{Kite}_{i,d} \le \bar{NT}^{Kite}_{i,d} - \left[\sum_{(i_o,d_o)\in OL^{Kite|Wind}_{i,d}} \left(y^{Wind}_{i_o,d_o}\ ROL^{Kite|Wind}_{(i,d)|(i_o,d_o)} \left(\frac{PD^{Kite}_{i,d}}{PD^{Wind}_{i_o,d_o}} - SL^{Kite|Wind}_{(d)|(d_o)} \right) \right) - \sum_{(i_o,d_o)\in OL^{Kite|Kite}_{i,d}} \left(\frac{1/PD^{Kite}_{i_o,d_o}\ y^{Kite}_{i_o,d_o}\ ROL^{Kite|Kite}_{(i,d)|(i_o,d_o)}}{1/PD^{Kite}_{i,d}} \right) \right] \qquad \forall\, d \in D_{Kite}, i \in I^d_{Kite} \tag{24}$$

The maximum radius for the energy collection system is limited by Eqs. (25)–(26) where OR_{v_i} is the set of designs that have their corresponding site location farther than R kilometers from the energy collection point associated with v_i. These constraints do not allow the transmission system to be larger than a certain radius, limiting the area where energy-harvesting devices may be deployed.

$$\sum_{(k,d)\in OR^{Wind}_{v_i}} y^{Wind}_{i,d} + \sum_{(k,d)\in OR^{Kite}_{v_i}} y^{Kite}_{i,d} \le (1 - v_i)\ \bar{NT} \quad \forall i \in I_{Tr} \tag{25}$$

Fig. 6. Flow chart showing the solution process of the portfolio optimization.

$$\sum_{i \in I_{Tr}} v_i = 1 \tag{26}$$

2.4. Portfolio optimization outputs

This subsection details the outputs of the portfolio optimization. In order to solve, the mixed integer nonlinear optimization is modeled in Pyomo [42,43]. It was then solved using Gurobi [44] as shown in Fig. 6.

The developed portfolio optimization selects the optimal configuration of candidate devices in order to coordinate energy generation from a variety of devices and/or resources for a given region of interest, subject to the constraints discussed in Section 2.3. To accomplish this, the model must consider each device's performance and costs at each location in the domain in order to calculate the energy sent back to shore and the LCOE. By using the input device models and environmental data, time series power for each site is calculated. It is then used with the input cost data for each device to determine the LCOE and the energy sent to shore. To provide meaningful analysis, the LCOE constraint is parameterized, and optimal configurations of devices are solved for at each LCOE to yield a full set of configurations. The best configuration in terms of energy delivered to shore is then selected and output. This process creates a computationally efficient frontier which captures the trade-offs between delivering more energy to shore, thereby displacing as much fossil fuel as possible, and decreasing LCOE so as to not drive the cost of energy upward.

3. Case study overview

This section lays out a case study using existing wind turbine models, optimized MHK kite designs, and a transmission system optimization model. The costs for candidate devices and the transmission system will be discussed in this section.

3.1. The North Carolina coast

This case study focuses on the offshore energy harvesting opportunities off of the coast of NC and explores the coordination of energy generation from wind turbines with a suite of optimized MHK kites. Environmental parameters such as wind speed and ocean current speed affect the amount of power that can be sent to shore and these change on a site-by-site basis. A map showing the wind speeds and ocean current speeds in the region of interest is shown in Fig. 7. The wind speed increases with distance from shore, and the ocean current speed increases within the Gulf Stream. It is noted that the ocean current speeds are minimal in areas that are not the Gulf Stream, and therefore have not been depicted.

Furthermore, water depth tends to increase with distance from shore, which affects transmission costs, due to transmission lines needing to be installed longer and deeper. Additionally, depth affects wind turbine and kite LCOEs predominantly due to mooring costs. Some of these costs can be alleviated when deploying kites off of floating platforms attached to the wind turbines themselves, which is why this deployment method was selected for this case study. Water depths for the domain are shown by contour lines in Fig. 7.

3.2. Transmission system costs

Estimates for the CapEx and OpEx of the transmission systems were made based upon Eqs. (27)–(37), which were derived from Faria et al. [18]. Eqs. (27)–(31) make up the CapEx of a AC system and represent the offshore platform and plant cost ($OPPC_{AC}$), the onshore plant cost (OPC_{AC}), the cost for reactive power compensation (CQ_{AC}), the cable cost (CC_{AC}), and the total CapEx ($CAPEX_{AC}^{TL}$), respectively. S_{TL} is the rated power of the transmission line, Q_c is the total reactive power produced by the line, N_c is the number of parallel circuits, cc_{AC}^{km} is the cost per kilometer of cable supply, ℓ_{TC} is the length of trunk cable, and D_{SL} is the distance of the energy collection point to shore.

Eqs. (32)–(35) represent CapEx of a DC system and represent the offshore platform and plant cost ($OPPC_{DC}$), the onshore plant cost (OPC_{DC}), the cable cost and installation (CC_{DC}), and the CapEx ($CAPEX_{DC}^{TL}$), respectively. Eq. (36) represents the OpEx of the system ($OPEX^{TL}$), and Eq. (37) represents the annualized transmission costs (TC^{TL}) where FCR^{TL} is the fixed charge rate.

The efficiency and LCOE (marginal component assuming 50% CF) for selected transmission configurations and the site locations considered in this work are shown in Fig. 8.

$$OPPC_{AC} = 6.55 + 0.0472\ S_{TL}\ [M\$] \tag{27}$$

$$OPC_{AC} = 0.03434\ {S_{TL}}^{0.7513}\ [M\$] \tag{28}$$

$$CQ_{AC} = 0.0262\ Q_c\ [M\$] \tag{29}$$

$$CC_{AC} = N_c cc_{AC}^{km} ell_{TC} + 0.221\ D_{SL} + 4.245x10^{-3}\ S_{TL} + 0.629\ [M\$] \tag{30}$$

$$CAPEX_{AC}^{TL} = OPPC_{AC} + OPC_{AC} + CQ_{AC} + CC_{AC}\ [M\$] \tag{31}$$

$$OPPC_{DC} = 32.75 + 0.07205\ S_{TL}\ [M\$] \tag{32}$$

$$OPC_{DC} = 0.1067\ S_{TL}\ [M\$] \tag{33}$$

$$CC_{DC} = N_c cc_{DC}^{km} \ell_{TC} + 0.221\ D_{SL} + 4.245x10^{-3}\ S_{TL} + 0.629\ [M\$] \tag{34}$$

$$CAPEX_{DC}^{TL} = OPPC_{DC} + OPC_{DC} + CC_{DC}\ [M\$] \tag{35}$$

$$OPEX^{TL} = 0.025\ CAPEX^{TL}\ [M\$/Year] \tag{36}$$

$$TC^{TL} = FCR^{TL} CAPEX^{TL} + OPEX^{TL}\ [M\$/Year] \tag{37}$$

3.3. Wind turbine costs

The capital and operational expenditures for these technologies are shown in Table 3 for fixed-bottom turbines at different water depths and site-to-landfall distances [31]. Wind speeds at 100, 140, and 160 m height were taken for the regions of interest in this case study from NREL Wind Toolkit at a maximum depth of 1000 m from January 2009 to December 2013 with spatial resolution of 2 km × 2 km and a 1-hour time discretization [26]. These speeds were adjusted to the wind turbine model hub heights using the wind profile power law [45]. This data combined with the CapEx and OpEx, enabled solving for capacity factors (CF) and LCOEs for these turbine models. The CFs and LCOEs for

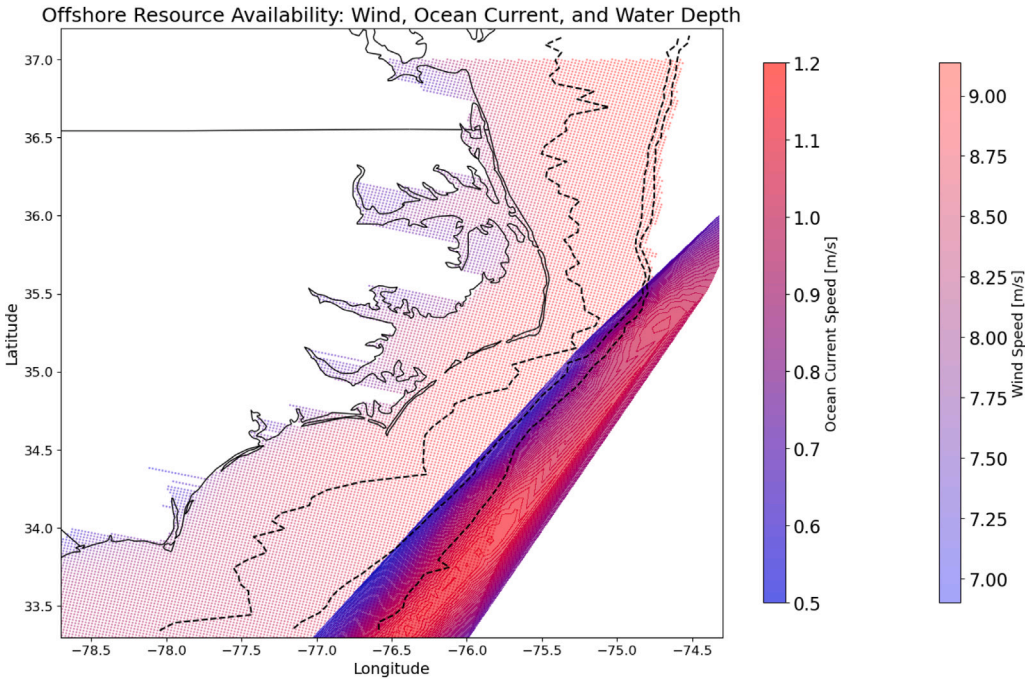

Fig. 7. Average ocean current speeds based on a 3-hour time discretization for 2007–2013 [27] overlaid onto average offshore wind speeds (2009–2013) off the coast of NC for a wind turbine with 140 m hub height [26]. Dashed lines represent different water depths.

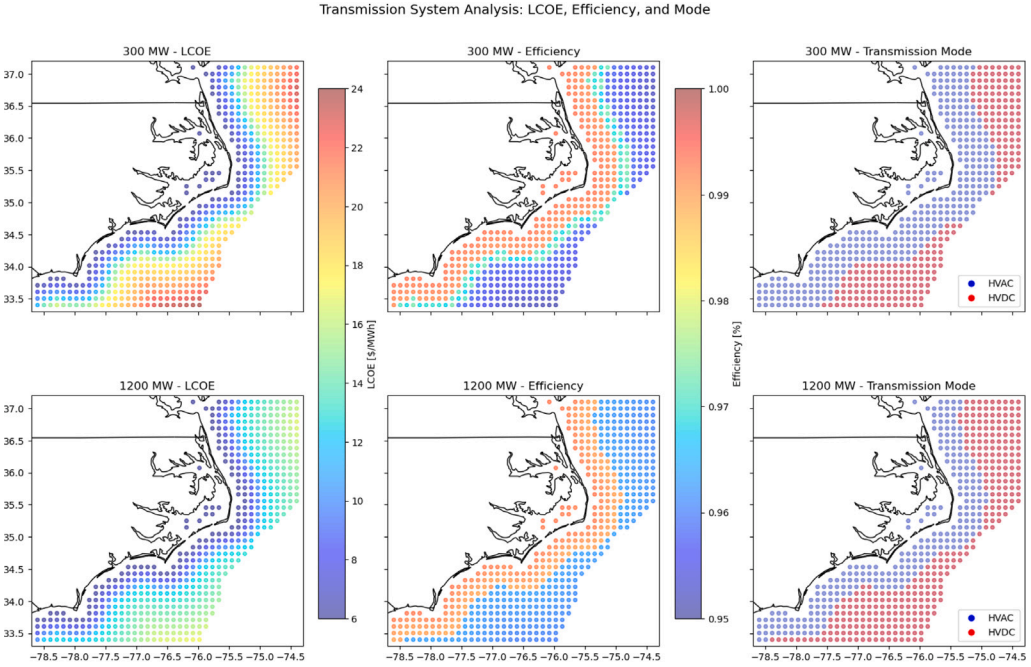

Fig. 8. Transmission system LCOE (assuming a 50% CF), efficiency, and mode of transmission (HVAC or HVDC).

8 and 18 MW wind turbines are shown in Fig. 9. CFs and LCOEs for 12 and 15 MW wind turbines are located in Appendix B. Higher capacity factor locations lend themselves to producing closer to the maximum theoretical energy of the device. Additionally, it is clear that the LCOE increases with distance from shore, despite high CFs, which indicates that mooring costs are a significant cost influence. Mooring costs are expected to increase with distance from shore due to increased water depth.

3.4. Kite costs

To select kite designs for input into the portfolio optimization, this work collected data from The Hybrid Coordinate Ocean Model (HYCOM) [27] at 3-hour time discretizations and 1/12° grid resolution for the time period 2009–2013. This data gets input into a control module which outputs the optimal time series power generation of a given kite in a given site location. This control module accounts for

Table 3
CapEx and OpEx estimates for fixed-bottom offshore wind turbines at different depths and distances from shore [31]. Here, TRG is representative of different ocean sites.

Resource group	Depth (m)	Site to landfall (km)	Base 2021 8 MW (102 m Hub)		Conservative 2030 12 MW (136 m Hub)		Moderate 2030 15 MW (150 m Hub)		Advanced 2030 18 MW (161 m Hub)	
			Capex [$/kW]	Opex [$/kW-yr]	Capex [$/kW]	Opex [$/kW-yr]	Capex [$/kW]	Opex [$/kW-yr]	Capex [$/kW]	Opex [$/kW-yr]
TRG 1	23	35	$3871	$118	$2435	$105	$2435	$87	$2435	$79
TRG 2	24	38	$3917	$121	$3357	$107	$2723	$89	$2464	$80
TRG 3	28	40	$4073	$123	$3397	$109	$2755	$90	$2562	$82
TRG 4	32	45	$4229	$124	$3533	$110	$2865	$91	$2660	$82
TRG 5	32	65	$4438	$127	$3668	$113	$2975	$94	$2792	$85
TRG 6	33	74	$4406	$126	$3849	$111	$3122	$92	$2772	$84
TRG 7	36	77	$4446	$120	$3822	$106	$3100	$88	$2797	$80

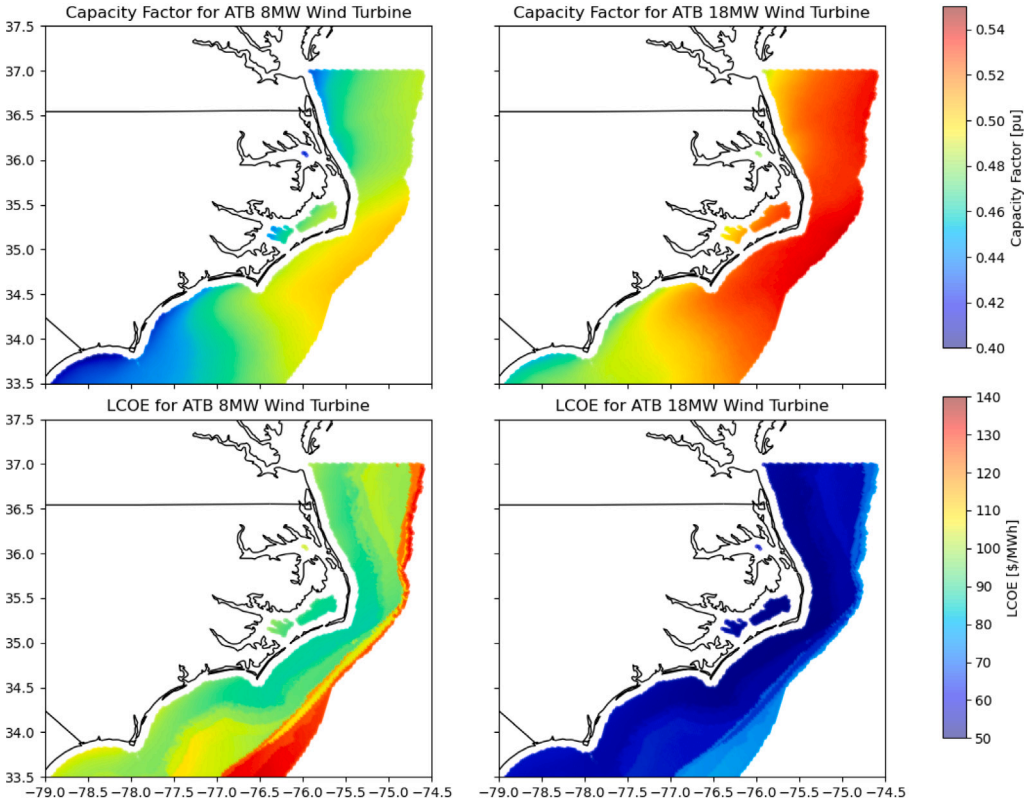

Fig. 9. Capacity factors and LCOEs for 8 and 18 MW wind turbine designs at different locations on the north carolina coast. Computed for The Period (2009–2013).

the changing ocean current profile causing the kite to adjust its depth in order to take advantage of relatively higher flows. The depth controller portion of this control model comes from [25]. It should be noted that although each kite was designed for a set depth, it is capable of operating at other depths, and adjusting depth is typical for kite systems. However, despite the possibility that the kite enters a zone in which the flow speed is high enough to generate more than its rated power, the kite is not permitted to generate more power than its rated power due to structural limitations.

The five kite designs with the most potential in terms of LCOE off the coast of NC were selected for use within this case study and are shown in Table 4. These five designs indicate that for this domain, the 147.47 kW kite design is the cheapest configuration at 23.49 $/MWh and the 931.91 kW design is still relatively cost-competitive at 39.90 $/MWh;

For each kite design, annualized cost estimates were developed. The ARPA-E SHARKS cost modeling spreadsheet [46] was used as the base for the calculations. Equations from the spreadsheet were adapted using kite sizing and cost modeling from Aull et. all, [47] with modifications to address variations between marine vs. airborne kites,

Table 4
Top five design configurations with the lowest average 10% LCOEs.

Design number	Design parameters		[a]Average 10% lowest LCOEs [$/MWh]
	Rated flow speed [m/s]	Rated power [kW]	
1	0.75	147.47	23.49
2	1	312.61	23.86
3	1.25	191.68	28.49
4	0.5	53.75	30.06
5	1.5	931.91	39.90

[a] Not considering transmission system cost.

such as increased costs of mooring and anchoring. Fig. 10 shows the CFs for a selection of kite designs, and Fig. 11 displays the corresponding LCOEs without accounting for transmission system costs, only showing LCOEs for sites below a threshold of 250 $/MWh. Based on these figures, a trend emerges. Sites with lower LCOEs tend to have higher CFs. This is because the higher the CF, the more often the device is generating power at capacity, hence increasing the devices power

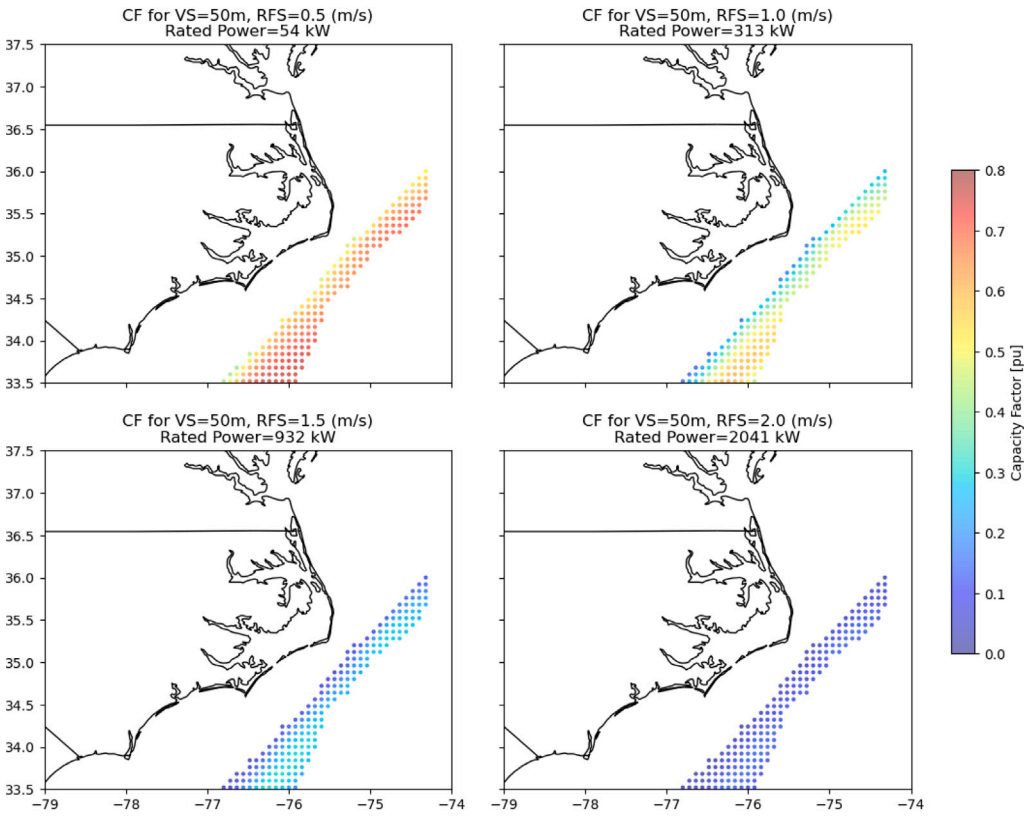

Fig. 10. CFs for selected kite designs with defined VS and rated flow speeds. Computed for the period 2009–2013.

output, which decreases LCOE. These sites with high CFs and low LCOEs also correspond to locations in the water column where the ocean current is on average, higher; this allows the kites to generate more power on average which increases CF, and decreases LCOE.

4. Case study results and discussion

This section investigates the power and LCOE implications of the proposed fused portfolio optimization model by exploring deployments of wind turbines and optimized MHK kites within the same transmission system. The chosen region of interest is off the entire coast of North Carolina, where the ocean current is conducive to kite deployment, and the wind resource is prominent. It was found that integrating the optimized suite of kites into the portfolio enables greater power generation at lower costs than single-device portfolios; avoiding the diminishing returns that accompany single-device systems. This is shown in Fig. 12 for a transmission system with a rated power of 300 MW, and in Fig. 13 for a transmission system with a rated power of 1200 MW, although this trend holds for all investigated transmission system rated powers.

For these efficient frontiers, optimal deployments were selected via the portfolio optimization model based upon a sweep of LCOE constraints. For the 300 MW efficient frontiers, it can be seen that the optimized suite of kites (blue, dashed line) outperforms the single device wind deployments (black and yellow lines) based strictly on LCOE, demonstrating a benefit of the portfolio optimization being able to choose the optimal design on a site-by-site basis. This occurs due to the kites having significantly lower LCOEs compared to wind turbines within this transmission system. Kites having lower LCOEs than wind turbines is especially significant for the 1200 MW transmission system and 8 MW wind turbines (increased base transmission costs compared to 300 MW). It is shown that the lowest attainable LCOE with only 8 MW wind turbines is higher than the attainable LCOE when combining kites and 8 MW turbines. This is due to the kites reducing the total LCOE by increasing power outputs at reduced costs. This is shown by the green line in Fig. 13. Note that the same effect does not occur for the 1200 MW transmission and 18 MW turbines due to the 18 MW turbines having lower LCOEs than kites under this transmission system. However, both the 300 MW and 1200 MW efficient frontiers show that the coordinated deployments of 8 MW and 18 MW wind turbines and the suite of kites (green and red lines) are able to achieve higher average powers sent back to shore at lower costs than single device deployments. Any reductions in average power along the frontiers for certain lower LCOEs are due to the configuration's location having to be balanced between being beneficial for kites and beneficial for wind turbines.

Fig. 14 shows the optimized deployment locations from the lowest LCOE condition from the 8 MW wind and kites deployment from Fig. 12 (green line). From the figure, it can be seen that the portfolio optimization chooses to place the devices where MHK kites can stretch as far into the gulf stream as possible, where the ocean current resource is the strongest, while still allowing the system radius to stretch close enough to shore that the water depth is conducive to wind turbine deployment. This relates back to Fig. 9, where it is shown that capacity factors become more favorable as distance to shore increases, because the depth also increases, the cost of mooring increases, making the LCOEs at these sites unfavorable. These selections from the portfolio optimization account for the combined deployment's ability to maximize power sent back to shore via its transmission system with low increases in LCOE; from the corresponding efficient frontiers, we can see that on average, our wind and kite deployments operate closer to the rated power of the transmission system that the individual device deployments the specific LCOE. Furthermore, it can be seen that different kites are selected by the portfolio on a site-by-site basis, allowing the kite deployments to operate in zones where their capacity factors are high, thereby reducing their LCOEs and enabling the suite of optimized kite designs to outperform the single-device wind turbine deployments.

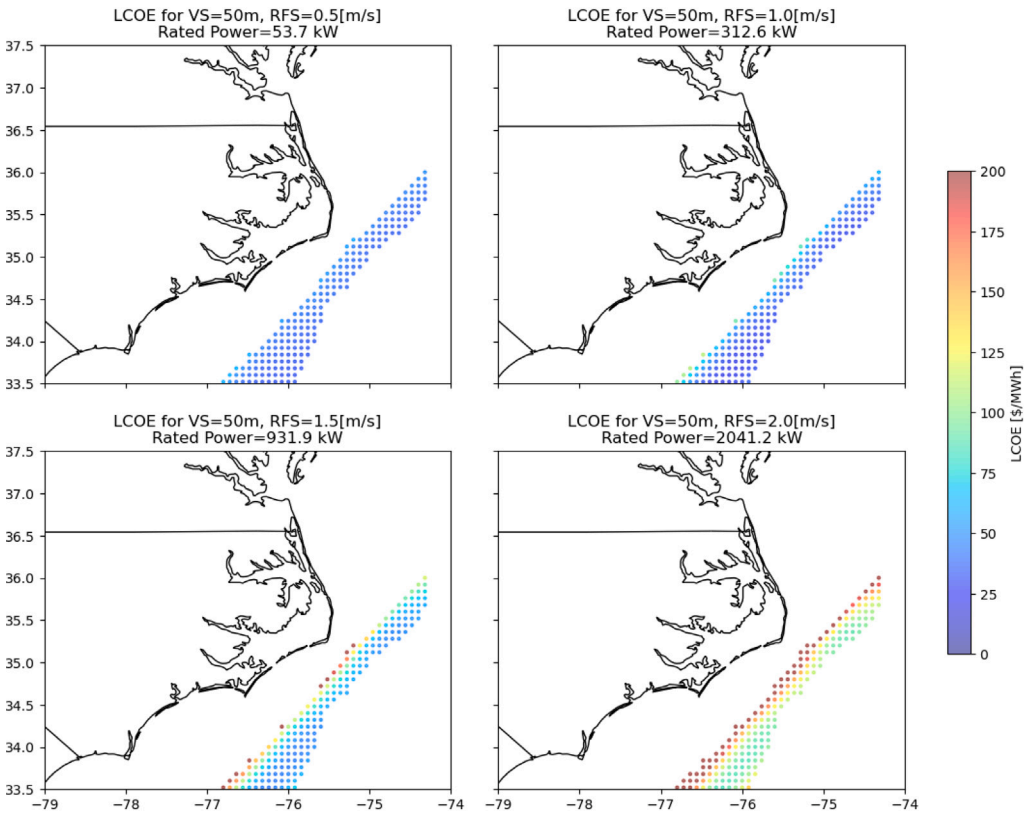

Fig. 11. LCOEs for a combination of kite designs developed with defined VS and rated flow speed. Values computed for the period 2009–2013.

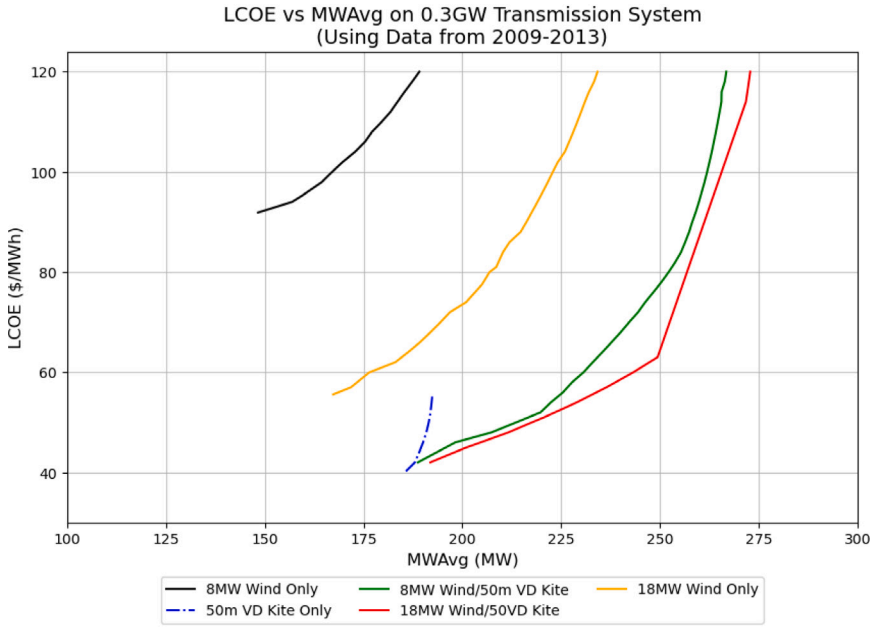

Fig. 12. Efficient frontiers for 300 MW transmission system: 8 MW wind turbine deployments (black), 18 MW wind turbine deployments (yellow), of optimized kite design suite deployments (blue, dashed), coordinated 8 MW wind turbine and optimized kite design suite deployments (green), and coordinated 18 MW wind turbine and optimized kite design suite deployments (red).

4.1. Sources of uncertainty and final remarks

It should be noted that there is inherently uncertainty in all cost and design models. Sources of uncertainty in cost models include changing costs of materials, labor, and permitting. Other evolving factors include government subsidies, grid demand, and stakeholder engagement, all of which may affect costs. A cost sensitivity study was performed in Fig. 15.

This study treats the 8 MW wind and kites scenario on a 300 MW transmission line, from Fig. 14, as the base case. It then varies

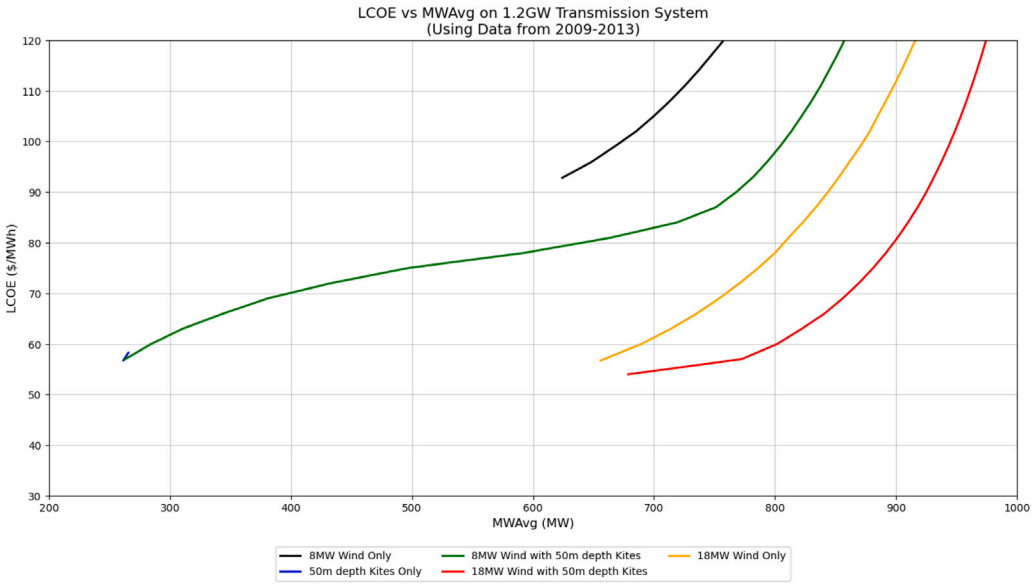

Fig. 13. Efficient frontiers for 1200 MW transmission system: 8 MW wind turbine deployments (black), 18 MW wind turbine deployments (yellow), of optimized kite design suite deployments (blue, dashed), coordinated 8 MW wind turbine and optimized kite design suite deployments (green), and coordinated 18 MW wind turbine and optimized kite design suite deployments (red).

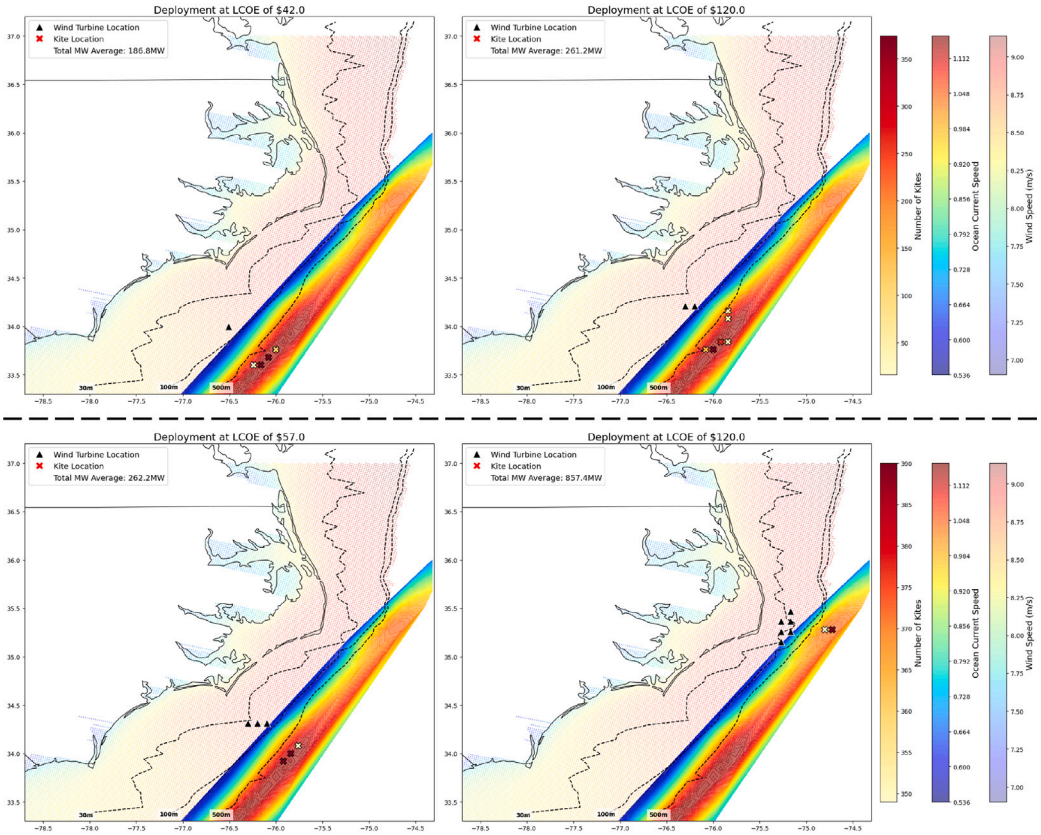

Fig. 14. Top: Deployment maps for the lowest and highest LCOE conditions from the 8 MW wind and kites deployment on 300 MW transmission system from Fig. 12 (green line). Bottom: Deployment maps for the lowest and highest LCOE conditions from the 8 MW wind and kites deployment on 1200 MW transmission system from Fig. 13 (green line). Wind and ocean current speeds are overlaid.

costs for wind, kites, and transmission individually by ±20%. From Fig. 15, it can be seen that reducing costs of wind, kites, and the transmission system reduces the LCOE for sending a given average power to shore. Similarly, increasing cost of wind turbines, kites, and the transmission system increases the LCOE for sending a given average power to shore. Interestingly, wind turbines are shown to be more sensitive to these effects. This is due to wind turbines having the highest baseline LCOEs. Another point of interest is that when the kite costs

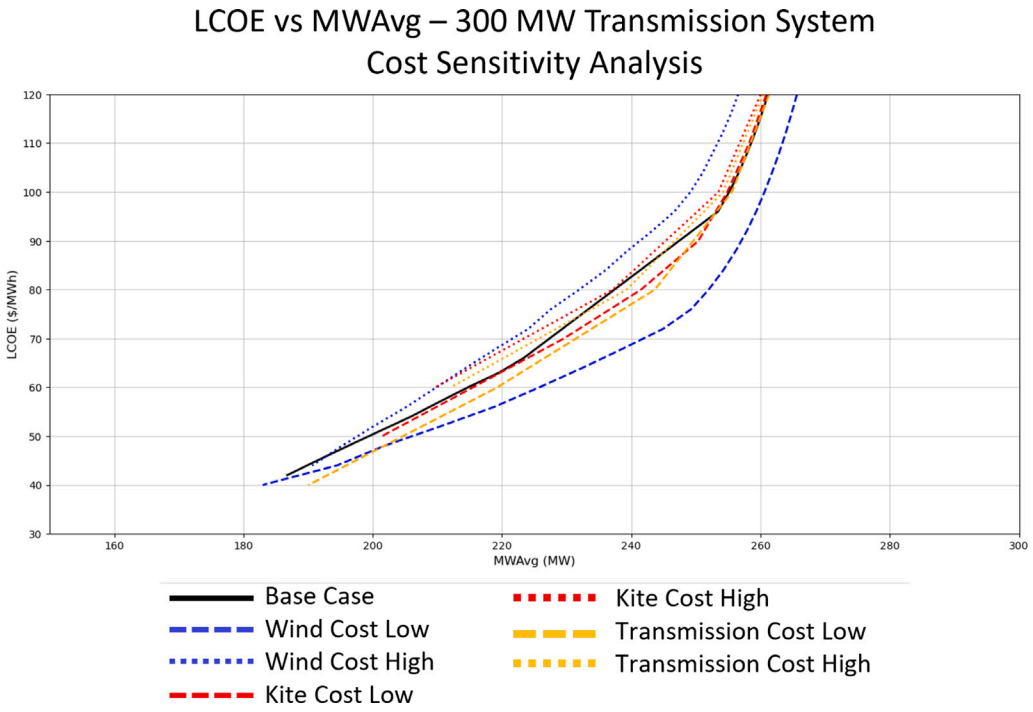

Fig. 15. These efficient frontiers represent various cost deviations from a baseline 8 MW wind and kite frontier. Blue dashed lines represent ±20% wind cost scenarios, red dashed lines represent ±20% kite cost scenarios, and yellow dashed lines represent ±20% transmission cost scenarios.

are varied, at higher LCOEs, these scenarios are almost identical. This indicates that at higher LCOE combined scenarios, wind turbines dominate power production. It should be noted that although this sensitivity study varied costs in terms of percentages, explicit quantification of cost model uncertainties should be of interest for continuing work. Furthermore, results will be affected by the fidelity of the optimized design library the user inputs to the portfolio optimization. Future work should include accounting for design model uncertainties, especially for designs of energy-harvesting devices that are in nascency and not yet being developed at full-scale.

5. Conclusion

This work introduced and tested a fused portfolio optimization model. This model integrated an optimized suite of energy-harvesting devices into a portfolio optimization model and expanded the portfolio optimization model to allow it to site-by-site select the best energy-harvesting device from a set of optimized devices. To enable the integration an optimized suite of energy-harvesting devices, a transparent MHK kite optimization model is contributed.

The case study of a domain off the coast of NC demonstrated that inputting suites of optimally designed energy harvesting devices into the portfolio optimization and allowing the model to decide which device designs are the best fit on a site-by-site basis enables coordinated deployments to send more power back to shore for minimal increases in LCOE. Furthermore, it clearly shows that deploying multiple offshore energy-harvesting devices in tandem on a shared transmission system enables the maximization of power transmitted back to shore in a cost-effective manner.

Future work should explore expansion of the portfolio optimization to include additional optimized suites of offshore energy-harvesting devices. With more optimized devices, it may be possible to gain additional power and cost benefits due to further diversification of the portfolio. Moreover, future work should address weighting terms to account for devices at lower innovation stages, capital discounts, and policy dynamics. Additionally, investigation of this optimization problem while addressing device model uncertainty, connecting the energy-harvesting configuration with energy storage, and addressing design of off-grid systems, like mobile energy harvesting devices are promising avenues to for the expansion of this work. Finally, future work should employ a systematic comparison of results from the portfolio optimization to hybrid energy systems, which may consist of different technologies from one another and exist in multiple domains.

CRediT authorship contribution statement

Mary Maceda: Writing – original draft, Software, Methodology, Investigation, Conceptualization. **Rob Miller:** Writing – review & editing, Visualization, Software, Investigation. **Victor A.D. de Faria:** Software, Methodology, Investigation, Conceptualization. **Matthew Bryant:** Supervision. **Chris Vermillion:** Writing – review & editing, Funding acquisition, Conceptualization. **Anderson R. de Queiroz:** Writing – review & editing, Project administration, Funding acquisition, Conceptualization.

Declaration of competing interest

The authors declare that they have no known competing financial interests or personal relationships that could have appeared to influence the work reported in this paper.

Acknowledgments

Funding: This work was supported by the North Carolina Renewable Ocean Energy Program (NCROEP), and administered by the Coastal Studies Institute, Wanchese, NC, with George Bonner as program manager. Any opinions, findings, conclusions or recommendations expressed in this material are those of the author(s) and do not necessarily reflect those of the NCROEP.

Appendix A. Optimized kite design analysis

Initially, at low flow speeds, the optimization model chooses a wing with a large span, and a small enough aspect ratio to allow

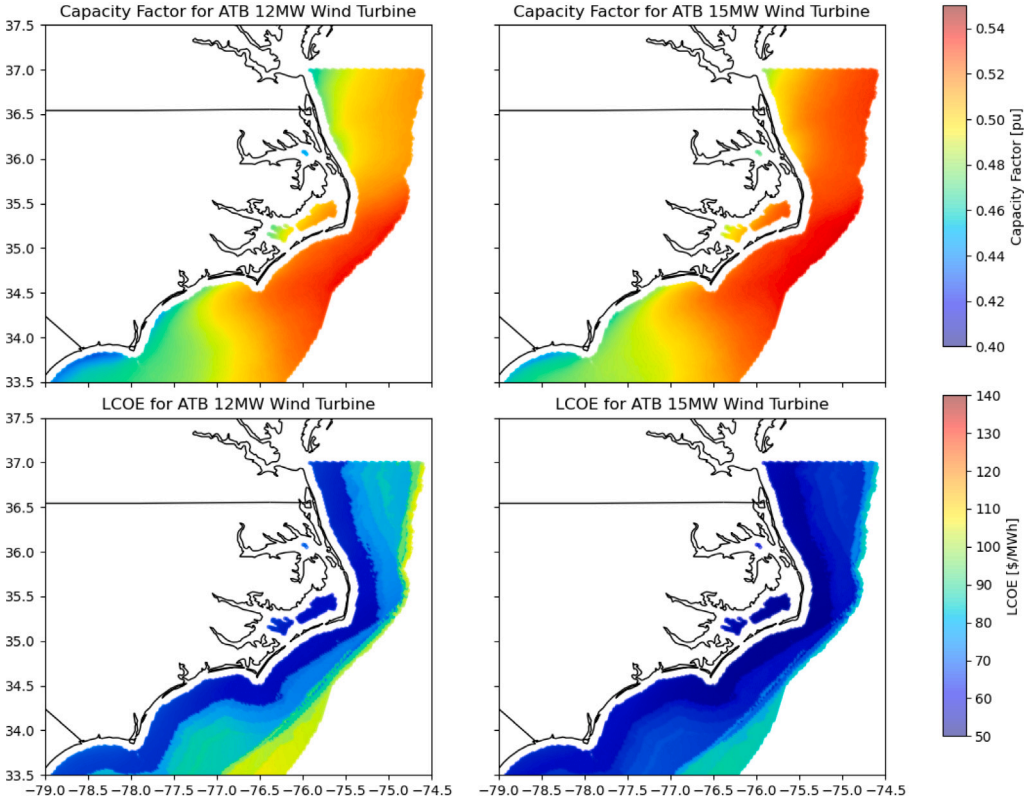

Fig. B.16. Capacity factors and LCOEs for 12 and 15 MW wind turbines at different locations on the North Carolina coast. Computed for The Period (2009–2013).

the wing enough surface area to achieve enough lift to maximize the extraction of power from the low flow. As the flow speed increases, the optimization selects a wing with high span and low aspect ratio to increase the surface area of the wing, thereby increasing the lift on the wing, which results in more power. This also increases the drag on the wing, which indicates that the drag of the kite is small in comparison to the tether drag, because if the drag of the kite were on the same scale as the drag from the tether, this increase in drag would greatly reduce power output. As the flow velocity continues to increase, the lift forces acting on the wing become too large to satisfy the structural constraints, most prominently the bending moment, thus the optimization opts for a wing with a lower span to reduce the bending moment. Furthermore, the power output of the kites increases with increasing flow speed due to the power being proportional to the prevailing flow speed cubed until the flow speed creates too much force on the wings such that structural constraints, namely bending moment, are no longer satisfied. The kite then reduces its span to reduce bending moment, which results in less lift for a given AR, and the kite being able to create less power.

The structural mass of the kite includes the internal spar structure, as well as the wing's outer shell and internal syntactic foam. Upon inspection of these results, it can be concluded that until 2.25 m/s flow speed, the kite's structural constraints are inactive, and the optimization selects the lower bound for the thickness of the wing shell. The required MOI increases as flow speed increases because high flow speeds result in higher forces on the wing, which results in this constraint becoming active with increasing flow speeds. To increase its bending rigidity, the structural mass in the kite increases at higher flow speeds. For further information on constraint activity in kites, the reader is directed to [39].

Appendix B. Capacity factors and levelized costs of energy for 12 and 15 MW wind turbines

See Fig. B.16.

Data availability

Data will be made available on request.

References

[1] Khan MZA, Khan HA, Aziz M. Harvesting energy from ocean: Technologies and perspectives. Energies 2022;15(9):3456.
[2] Smith RF. Offshore wind potential in north carolina and possible configuratons (Ph.D. thesis), Reykjavik University; 2016.
[3] Haas K. Assessment of energy production potential from ocean currents along the United States coastline. Tech. rep., Georgia Institute of Technology, Atlanta, GA (United States); 2013.
[4] Global Wind Energy Council. Global offshore wind report 2020. GWEC: Bruss Belg 2020;19:10–2.
[5] Musial W, Spitsen P, Duffy P, Beiter P, Shields M, Mulas Hernando D, Hammond R, Marquis M, King J, Sathish S. Offshore wind market report: 2023 edition. Tech. rep., National Renewable Energy Laboratory (NREL), Golden, CO (United States); 2023.
[6] Kilcher L, Fogarty M, Lawson M. Marine energy in the United States: An overview of opportunities. Tech. rep., NREL; 2021.
[7] Hass K. Assessment of energy production potential from ocean currents along the United States coastline. Tech. rep., Georgia Tech Research Corporation; 2013.
[8] General Assembly of North Carolina. House bill 951. 2021.
[9] Lowcher CF, Muglia M, Bane JM, He R, Gong Y, Haines SM. Marine hydrokinetic energy in the Gulf Stream off North Carolina: an assessment using observations and ocean circulation models. Mar Renew Energy: Resour Charact Phys Eff 2017;237–58.
[10] Faria VA, de Queiroz AR, DeCarolis JF. Scenario generation and risk-averse stochastic portfolio optimization applied to offshore renewable energy technologies. Energy 2023;270:126946.
[11] Markowitz H. Modern portfolio theory. J Financ 1952;7(11):77–91.
[12] Markowitz HM, Todd GP. Mean-variance analysis in portfolio choice and capital markets. Vol. 66, John Wiley & Sons; 2000.
[13] Neto DP, Domingues EG, Coimbra AP, de Almeida AT, Alves AJ, Calixto WP. Portfolio optimization of renewable energy assets: Hydro, wind, and photovoltaic energy in the regulated market in Brazil. Energy Econ 2017;64:238–50.
[14] Ahmadi SA, Mirlohi SM, Ahmadi MH, Ameri M. Portfolio optimization of power plants by using renewable energy in Iran. Int J Low-Carbon Technol 2021;16(2):463–75.

[15] Cucchiella F, Gastaldi M, Trosini M. Investments and cleaner energy production: A portfolio analysis in the Italian electricity market. J Clean Prod 2017;142:121–32.
[16] Mohammadi E, Karimi MH, Eskorouchi A, Ghanbari H. Dempster–Shafer-informed levelized cost of energy: A robust approach for energy portfolio optimization under deep uncertainty. Results Eng 2025;107756.
[17] Li B, de Queiroz AR, DeCarolis JF, Bane J, He R, Keeler AG, Neary VS. The economics of electricity generation from Gulf Stream currents. Energy 2017;134:649–58.
[18] de Faria VA, de Queiroz AR, DeCarolis JF. Optimizing offshore renewable portfolios under resource variability. Appl Energy 2022;326:120012.
[19] Jamaleddin N, de Faria V, de Queiroz A, Gabr M. Optimizing co-located offshore wave and wind energy systems: Feasibility, design, and portfolios assessment. J Clean Prod 2025;523:146461.
[20] Sun X, Huang D, Wu G. The current state of offshore wind energy technology development. Energy 2012;41(1):298–312.
[21] North Carolina Governor Roy Cooper. Executive Order No. 218, "Advancing North Carolina's Economic and Clean Energy Future with Offshore Wind". 2021.
[22] Projects. 2025, URL https://minesto.com/projects/, [Online; Accessed Feburary 2025].
[23] Loyd ML. Crosswind kite power (for large-scale wind power production). J Energy 1980;4(3):106–11.
[24] Kite systems. 2024, URL https://minesto.com/products/kite-systems, [Online; Accessed Feburary 2024].
[25] Naik KP, Vermillion C. Integrated plant, site, and control system co-design for an underwater energy-harvesting kite system. In: Site, and Control System Co-Design for an Underwater Energy-Harvesting Kite System. 2023.
[26] Wind integration national dataset toolkit. Tech. rep., National Renewable Energy Laboratory; 2023, [Online; Accessed June 2023].
[27] HYCOM. GOFS 3.1: 41-layer HYCOM + NCODA glabal 1/12 °. 2022, [Online; Accessed June 2022].
[28] LiVecchi A, Copping A, Jenne S, Gorton A, Preus R, Gill G, Robichaud R, Green R, Geerlofs S, Gore S, et al. Powering the blue economy: Exploring opportunities for marine renewable energy in various maritime. Tech. rep., National Renewable Energy Laboratory (NREL), Golden, CO (United States); 2019.
[29] Neary VS, Lawson M, Previsic M, Copping A, Hallett KC, Labonte A, Rieks J, Murray D. Methodology for design and economic analysis of marine energy conversion (MEC) technologies. 2014.
[30] Bhuiyan MA, Hu P, Khare V, Hamaguchi Y, Thakur BK, Rahman MK. Economic feasibility of marine renewable energy. Front Mar Sci 2022;9:988513.
[31] Annual Technology Baseline. Tech. rep., National Renewable Energy Laboratory; 2022, [Online; Accessed June 2023].
[32] dos Santos Ferreira OM. Emerging renewable energy technologies: Survey, modeling, and simulations. 2020.
[33] Trevisi F, McWilliam M, Gaunaa M. Configuration optimization and global sensitivity analysis of ground-gen and fly-gen airborne wind energy systems. Renew Energy 2021;178:385–402.
[34] Diehl M. Airborne wind energy: Basic concepts and physical foundations. In: Airborne wind energy. Springer; 2013, p. 3–22.
[35] Reed J, Naik K, Abney A, Herbert D, Fine J, Vadlamannati A, Morris J, Taylor T, Muglia M, Granlund K, et al. Experimental validation of an iterative learning-based flight trajectory optimizer for an underwater kite. IEEE Trans Control Syst Technol 2024;32(4):1240–53.
[36] Abney A, Fine J, Vermillion C. Drag-mitigating dynamic flight path design and sensitivity analysis for an ultra-long tether underwater kite. J Dyn Syst Meas Control 2025;147(1).
[37] Costello S, Costello C, François G, Bonvin D. Analysis of the maximum efficiency of kite-power systems. J Renew Sustain Energy 2015;7(5).
[38] Stengel RF. Flight dynamics. Flight Dynamics. Second ed.. Princeton University Press; 2022,
[39] Maceda M, Bryant M, Vermillion C. Implications of structural and buoyancy constraints on the design of marine hydrokinetic energy-harvesting kites. In: OCEANS 2024-halifax. IEEE; 2024, p. 1–9.
[40] Fine JB, McGuire CM, Reed J, Bryant M, Vermillion C. Optimal cyclic control of a structurally constrained span-morphing underwater kite in a spatiotemporally varying flow. In: 2023 American control conference. ACC, IEEE; 2023, p. 2084–90.
[41] Roylance D. Pressure vessels. Cambridge: Department of Materials Science and Engineering, Massachusetts Institute of Technology; 2001.
[42] Hart WE, Watson J-P, Woodruff DL. Pyomo: modeling and solving mathematical programs in Python. Math Program Comput 2011;3(3):219–60.
[43] Bynum ML, Hackebeil GA, Hart WE, Laird CD, Nicholson BL, Siirola JD, Watson J-P, Woodruff DL. Pyomo–optimization modeling in Python. third ed.. Vol. 67, Springer Science & Business Media; 2021.
[44] Gurobi Optimization, LLC. Gurobi optimizer reference manual. 2024, URL https://www.gurobi.com.
[45] NOAA. LLLJP wind shear formula (power law). 2014, [Online; Accessed June 2023].
[46] ARPA-E. Submarine hydrokinetic and riverine kilo-megawatt systems (sharks). 2024, [Online; Accessed April 2024].
[47] Aull M, Stough A, Cohen K. Design optimization and sizing for fly-gen airborne wind energy systems. Automation 2020;1(1):1–16.